JGR Oceans

RESEARCH ARTICLE
10.1029/2019JC015420

Small-Scale Topographic Form Stress and Local Dynamics of the Southern Ocean

Xihan Zhang[1,2] and **Maxim Nikurashin**[1,2,3]

[1]Institute for Marine and Antarctic Studies, University of Tasmania, Hobart, Tasmania, Australia, [2]ARC Centre of Excellence for Climate Extremes, Hobart, Tasmania, Australia, [3]Australian Antarctic Program Partnership, Institute for Marine and Antarctic Studies, University of Tasmania, Hobart, Tasmania, Australia

Key Points:
- The effect of abyssal hills is for the first time explicitly simulated in an internal wave-permitting regional ocean model
- Abyssal hills generate strong topographic form stress comparable with that from large-scale topography
- Abyssal hills modify the vertical structure and meanders of the ACC and contribute significantly to the equilibration of transient eddies

Correspondence to:
Correspondence to: X. Zhang,
xihan.zhang@utas.edu.au

Citation:
Zhang, X., & Nikurashin, M. (2020). Small-scale topographic form stress and local dynamics of the Southern Ocean. *Journal of Geophysical Research: Oceans*, *125*, e2019JC015420. https://doi.org/10.1029/2019JC015420

Received 27 JUN 2019
Accepted 2 MAY 2020
Accepted article online 8 MAY 2020

Abstract The contribution of small-scale abyssal hill topography to the topographic form stress and local dynamics of the Southern Ocean is investigated using a high-resolution model of the sector of the Southern Ocean south of Tasmania and New Zealand. The results of two simulations, with and without small, O(1–100 km), scale topography, confirm that the effects of small-scale topography are exerted through the generation of strong topographic form stress leading to transient eddy dissipation and changes in flow meanders. Small-scale topographic form stress is comparable in magnitude to that generated by large-scale topography, but with a pairwise distribution of positive and negative stress values upstream and downstream of the Macquarie Ridge, consistent with the meandering of the flow. In the experiment without small-scale topography, the bottom mean flow speed increases, while the surface mean speed slightly decreases, making the mean flow more barotropic. Eddy kinetic energy also greatly enhances throughout the water column after removing small-scale topography. Our results suggest that small-scale topography has strong impact on transient eddies and plays an important role for setting the vertical structure of the flow and the equilibration and position of flow meanders.

1. Introduction

The absence of the latitudinal boundaries and vigorous westerly winds in the Southern Ocean allow the formation of the Antarctic Circumpolar Current (ACC). It is pivotal in the ocean circulation, providing an inter-basin connection between the major oceans and permitting the advent of a global overturning circulation. Therefore, it promotes the exchange of heat, fresh water, and other tracers between ocean basins, surface and abyssal ocean, and oceans and the atmosphere and thus plays a prominent role in climate (e.g., Rintoul et al., 2001; Rintoul & Naveira Garabato, 2013). Driven by constant and strong westerly wind over the Southern Ocean, the ACC flows persistently eastward around Antarctica. Without the continental boundaries required to remove wind-input momentum in closed ocean basins, the momentum budget of the ACC is closed through other dynamical processes in which the dominant one is the topographic form stress (TFS) associated with pressure differences across topographic features (Munk & Palmén, 1951).

The momentum balance of the ACC has been previously investigated in various models. In an early coarse-resolution numerical model, Gill and Bryan (1971) found that the introduction of topography influenced the transport and dynamical processes of the ACC due to the occurrence of cross-topographic pressure gradient. A series of eddy-permitting models were then used to estimate the further effect of TFS. McWilliams et al. (1978) found that the transport of the ACC decreased to a value comparable with observations when the two-layer quasi-geostrophic model they used included topographic obstacles. This revealed that instead of friction near the bottom, it is the TFS that removes the momentum input by wind, confirming the validity of the momentum balance mechanism proposed by Munk and Palmén (1951). Similar results were later obtained by other numerical experiments including quasi-geostrophic models (Marshall et al., 1993; Wolff et al., 1991) and the Fine Resolution Antarctic Model (FRAM) (Ivchenko & Stevens, 1995; Ivchenko et al., 1996; Killworth & Nanneh, 1994).

A more recent estimate of the effect of TFS was undertaken in a 1/6° eddy-permitting Southern Ocean State Estimate (SOSE) model (Masich et al., 2015), which indicated that when integrated zonally, TFS can balance wind stress at each latitude with shallow ridges and South America contributing most toward the westward momentum. Pressure gradient in the depth-integrated momentum balance consists of interior and bottom

pressure difference. The major difficulty overcome in Masich et al. (2015) was separating the local TFS contribution (due to pressure difference across topography) from the contribution of the pressure gradient in the ocean interior, the approach we follow in our study.

The role played by small, O(1–100 km), scale topography in the momentum balance of the ACC has been recently theoretically evaluated by Naveira Garabato et al. (2013) utilizing a linear internal wave theory. They related the small-scale TFS with internal lee waves generated by topographic features of horizontal scales roughly from 1 to 10 km. Unlike large-scale topography where flows go around, the cross-topographic pressure gradient associated with small-scale topography is mainly generated when flows go over the small obstacles (Bell, 1975). The vertical flux of horizontal momentum then arises on the condition that these perturbations, which are also known as internal lee waves, can radiate away. Concurrent with the formation of radiating internal lee waves, the internal wave drag is applied on the background flow and energy is extracted from it to power the wave radiation. This wave drag was also noted as small-scale TFS and was estimated in theory in Naveira Garabato et al. (2013). The results showed that although the small-scale TFS plays a minor role on the global scale, it can be a notable local momentum source or sink over regions where the small-scale topography has large variability, especially over the regions of the ACC. These results have recently been extended to lee wave drag and energy extraction from transient eddies in a similar offline calculation by Yang et al. (2018). In addition to internal waves, the small-scale topography can generate other motions including evanescent internal waves and topographic wake eddies also contributing to TFS (Klymak, 2018).

Consistent results were obtained using altimetry and a 1/4° resolution general circulation model with a realistic topography (Gille, 1997). By comparing the altimeter data with the model outputs, Gille (1997) found that in addition to the three large-scale topographic features (Kerguelen Island, Campbell Plateau, and Drake Passage) evaluated in the model, smaller topographic obstacles can generate TFS as well and they also had an impact on the ocean surface, which was not captured in the numerical model due to the resolution limitation. This result implied the importance of the understanding of small-scale TFS. This conclusion, to some degree, aligns with the prior studies which suggested that the enhancement of internal wave energy and turbulent dissipation occur consistently in regions where the ACC flows over small-scale topography (e.g., Kunze et al., 2006; Naveira Garabato et al., 2004; Sloyan, 2005).

The importance of small-scale topography may also be embodied in the mechanism of the ACC responding to changes of westerly winds. Using observations, Böning et al. (2008) showed that isopycnals in the ACC are insensitive to winds, suggesting that the baroclinic transport remains stable even though wind forcing has increased in the past decades. This has motivated a series of studies, and one of them is from Thompson and Naveira Garabato (2014), who proposed an explanation for this insensitivity based on standing meanders. By capturing barotropic Rossby waves triggered by large-scale topographic features, the ACC flow therefore flexes, forming standing meanders (Hughes, 2005), which have been suggested to play an important part in a mechanism for the downward transfer of the momentum input by wind. According to Thompson and Naveira Garabato (2014), as wind stress varies, the curvature of meander changes correspondingly, thus adjusting the barotropic vorticity balance to transfer the changing momentum to the bottom, where it is balanced, leading to the insensitivity of the ACC. The curvature variation in a meander was found to be correlated to the elevated bottom speed, which was conjectured to be the cause of associated increased energy dissipation through friction or more likely the generation of internal lee waves and therefore implies the importance of the small-scale topography in the dynamics of the ACC.

Due to the model resolution limitation, the effect of small-scale bottom topography has not been analyzed in simulations explicitly resolving small-scale topography. In this study, to investigate the role played by small-scale topography in the ACC, we use a fine-resolution numerical simulation of the Southern Ocean circulation which can directly resolve not only the topographic features with horizontal scale of O(1 km) but also the internal lee waves and other small-scale motions generated by them. TFS is expected to be explicit in this model resulting from both small- and large-scale topography. To explore this TFS locally, we follow the TFS calculation method proposed by Masich et al. (2015). Additionally, to further investigate the dynamics of the ACC based on the mechanism of the vertical transfer of horizontal momentum proposed by Thompson and Naveira Garabato (2014), we complement their study by keeping the wind steady, but varying small-scale topography and evaluating the resulting changes in the TFS, bottom flow speed, and flow menders.

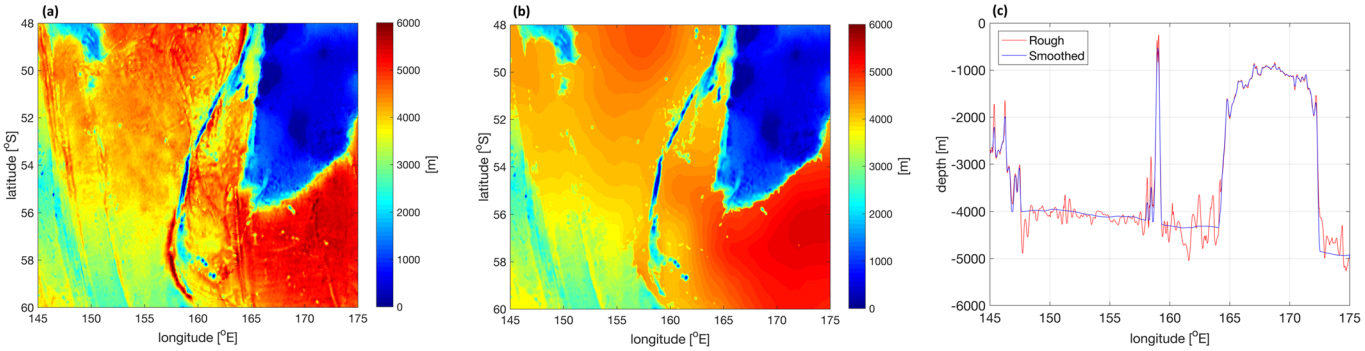

Figure 1. Bathymetry in (m) from (a) rough topography experiment and (b) smooth topography experiment. (c) Topography depth (m) comparison at 54°S between rough and smooth topography simulation.

This paper is structured as follows. Section 2 describes the model configuration and the perturbation experiment, along with various diagnostics we use to evaluate the flow changes with small-scale topography. Results of the reference model and the perturbation experiment are presented in section 3 and followed by the discussion and conclusions in section 4.

2. Methods

2.1. Model Configuration and Experiments

In this study, we use the primitive equation Massachusetts Institute of Technology general circulation model (MITgcm) (Marshall et al., 1997) to simulate the regional circulation of the Southern Ocean. Similar model configurations have been employed and validated in previous studies (e.g., Mashayek et al., 2017; Rosso et al., 2014, 2015; Tulloch et al., 2014).

The ACC region we simulate is south of Tasmania and New Zealand (145–175°E, 48–60°S) (Figure 1a). We apply open boundary conditions with the steady annual-mean fields of velocities, temperature, and salinity from the SOSE (Mazloff, 2005). The circulation is restored to open boundary condition in the sponge layers with about 1° width at all lateral boundaries. Surface temperature and salinity are restored to annual-mean fields with a 10-day restoring time scale. The sea surface is configured to be a free surface, and the free-slip boundary condition is used on all boundaries. A quadratic drag is implemented at the bottom with a drag coefficient of 0.002. All the simulations are driven by annual-mean wind stress also taken from SOSE. The equation of state is the UNESCO formula with a horizontally uniformed and steady pressure modified by Jackett and Mcdougall (1995).

Our reference simulation has 1/80° resolution with the horizontal grid size of about 800 m. We use 200 vertical levels which vary from 4 m at the surface to 40 min the deep ocean uniform below 2-km depth. The maximum depth is 6 km. This resolution is fine enough to resolve the dominant internal lee waves which have horizontal scales of a few kilometers and vertical scales of a few hundred meters (e.g., Nikurashin & Ferrari, 2011; Scott et al., 2011). Bathymetric data are the Shuttle Radar Topography Mission, SRTM30_PLUS, bathymetry with 1/120° resolution (Becker et al., 2009; Sandwell & Smith, 2009). Model outputs are stored every 5 days during the 4-month simulation, and the analysis is based on the outputs from the last 3 months after the spin-up and equilibration. Although the simulated period is only 4 months, the model at 1/80° resolution equilibrates after about 1 month, because it is initialized from a well-equilibrated 1/20° resolution model that was run for 10 years.

In order to investigate the role of small-scale topography, we carry out simulations with and without small-scale topography. In the simulation without small-scale topography, the bathymetric data deeper than 3.5 km are smoothed using the running mean with the averaging scale of about 100 km so that the deep small-scale topography is removed, while large-scale deep and all shallow topography remains the same. Bathymetry of simulated region for both simulations is shown in Figure 1. Bathymetry profile along 54°S is plotted in Figure 1c in which both large-scale and small-scale topography can be easily seen. The

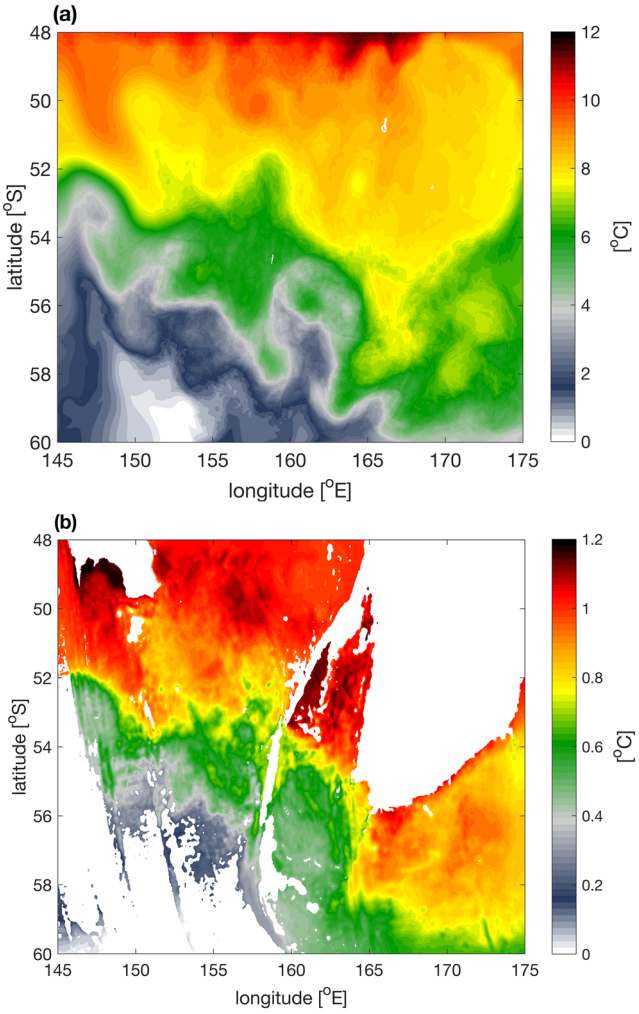

Figure 2. Time-mean temperature in (°C) from the reference experiment (a) at the surface and (b) at 3,500-m depth.

smoothed-topography model is also run at 1/80° resolution and compared with the 1/80° reference model simulation. We also refer to our reference simulation as *Rough* and to the simulation without small-scale topography as *Smooth*below.

The simulated region is a part of Macquarie fault zone. The narrow strip in the middle of the domain is the Macquarie Ridge. It extends to approximately 1,500 m on average below the surface in the vertical and extends as far south as 56°S in the meridional direction, followed by a trough in the south. This ridge is one of the major obstacles hampering the ACC with a large portion of the ACC going through its narrow gap at 53°S (Gordon, 1972). The other extensive shallow area next to the Macquarie Ridge is the Campbell Plateau, most of which is shallower than 1,000 m, bounded by an abrupt slope dropping from 1,000 m to deeper than 4,000 m within about 10-km distance. These two large-scale topographic features have been shown to generate negative TFS that contributes to balancing the zonally averaged wind stress (Masich et al., 2015). In addition to these two major large-scale features, there are abyssal hills in this region both upstream and downstream of the Macquarie Ridge, most of which are removed in our smooth topography simulation. A part of the Balleny fracture zone can also be seen in the southwest of the domain. The region of our study is one of the eddy hotspots in the Southern Ocean with a flexing meander studied for local dynamics by Thompson and Naveira Garabato (2014).

2.2. Model Diagnostics

We use multiple diagnostics, such as time-mean flow, sea surface temperature, sea surface height, and eddy kinetic energy (EKE), to investigate the changes in the circulation in response to small-scale topography. To quantify the role of small-scale topography for the dynamical balance of the Southern Ocean, we also evaluate the TFS following the approach of Masich et al. (2015). Since our model is regional, the leading order vertically integrated momentum balance is between wind stress, Coriolis acceleration, and pressure gradient (e.g., Naveira Garabato et al., 2013). Masich et al. (2015) showed that, taking the circumpolar integral, the balance reduces to wind stress at the surface and TFS at the bottom. The TFS is a part of the integrated pressure gradient, that is,

$$\int_x \int_{z=-H}^{\eta} \frac{\partial p}{\partial x} dz dx = \int_x \left[\underbrace{-\frac{\partial}{\partial x} \int_{z=-H}^{\bar{\eta}} \bar{p}\, dz}_{(i)} + \underbrace{\overline{p_{atm}} \frac{\partial \eta}{\partial x}}_{(ii)} + \underbrace{\overline{p_b} \frac{\partial H}{\partial x}}_{(iii)} \right] dx, \tag{1}$$

where (*i*) is the interior pressure difference between the two latitudinal boundaries of the region; (*ii*) is the momentum input at the surface by the surface pressure p_{atm}, negligible compared to the effect of bottom pressure p_b; and (*iii*) is the zonal momentum transferred to the Earth by interfacial form stress, that is, TFS, vanishing if the bottom is flat. To quantify the TFS in (*iii*) in our regional model, we follow the numerical method proposed by Masich et al. (2015) which evaluates TFS by computing the pressure difference tied to each topographic feature and hence allows examining the spatial distribution of the TFS.

The method for calculating the TFS applies as follows. At each vertical model level, we take the time-mean bottom pressure difference between two edges of one single piece of topography (east minus west),

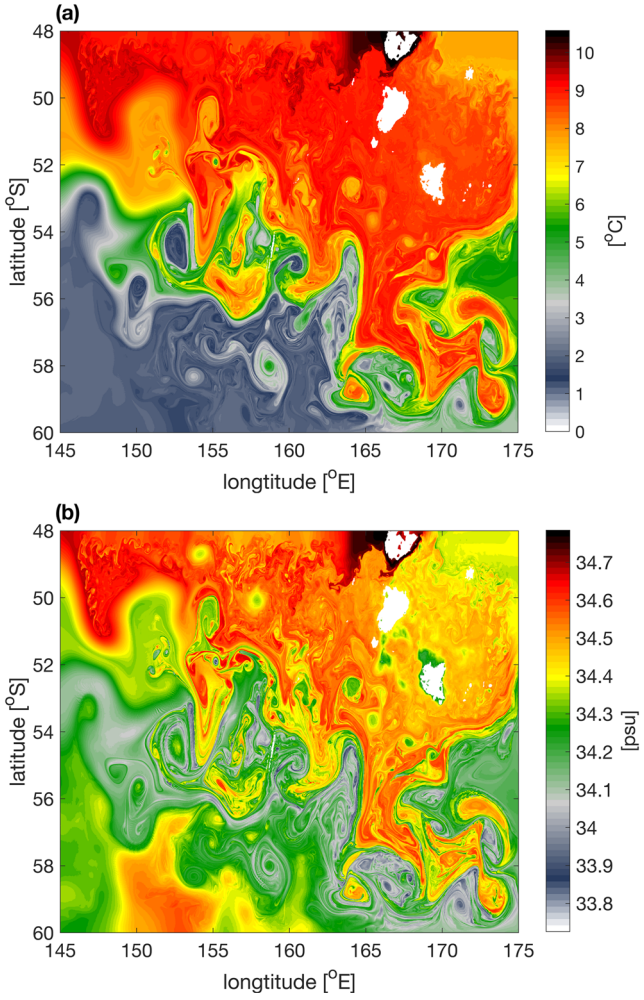

Figure 3. Snapshots of (a) temperature in (°C) and (b) salinity in (psu) at 200-m depth from the reference experiment.

$$\Delta\overline{p_b} = \overline{p_b}(x_E) - \overline{p_b}(x_W). \quad (2)$$

Then we divide $\Delta\overline{p_b}$ by the distance between the two pressure points, $\Delta x = x_E - x_W$, and integrate it vertically,

$$\sum_{z=-H}^{\bar{\eta}} \frac{\Delta\overline{p_b}}{\Delta x}\Delta z. \quad (3)$$

We only take into account the topography that has two sides in the model so that the pressure difference across that topography can be calculated. Topography with pressure only on one side represents a small fraction of the overall topography in this region and is ignored. We plot the maps of the TFS to compare the local form stress and its changes produced by varying motions as well as topographic features. The reader is referred to Masich et al. (2015) for a more detailed description of the method.

3. Results

3.1. Reference Simulation

The reference simulation, using unmodified 1/120° bathymetry data, resolves both realistic topographic features on the order of 1- to 100-km scale, characteristic of abyssal hills (e.g., Bell, 1975; Nikurashin & Ferrari, 2011; Scott et al., 2011), as well as internal lee waves, evanescent motions, topographic wakes, and other motions generated by these abyssal hills. Large-scale flows, mesoscale, and submesoscale eddies are also well resolved and simulated by the model as we demonstrate below.

The distribution of the time-mean temperature at the surface and 3,500-m depth is shown in Figure 2. The surface temperature delineates the large-scale meridional gradient across the domain, where the northernmost temperature is around 10–12°C and the southernmost temperature is around 0–2°C. The strong temperature gradient seen meandering between 52°S and 54°S corresponds to the Subantarctic Front (SAF) of the ACC. The SAF penetrates the deep ocean (Figure 2b), where we can observe its path (indicated by strong temperature gradient) flowing through the narrow gap of the Macquarie Ridge at 53°S and then along the bathymetry of the Campbell Plateau downstream. These two large-scale topographic features have been suggested to generate a Rossby wave, which tends to propagate westward and is arrested by the strong flow of the ACC, forming a standing meander around 150–155°E (Thompson & Naveira Garabato, 2014).

In addition to the large-scale and time-mean temperature gradient and associated circulation, there are small-scale and transient eddies simulated by the model, which also characterize the circulation in this region. Figure 3 shows snapshots of temperature and salinity at 200-m depth 15 days after the model equilibration, in which strong meanders and vigorous mesoscale and submesoscale eddies can be clearly seen. In the temperature snapshot, we can see the SAF meanders and transient eddies, including both warm-core and cold-core eddies. Similar features can be observed in the salinity snapshot. The pattern of the salinity gradient is largely in agreement with the temperature gradient across the ACC with higher salinity (around 34.6 psu) in the north and lower salinity (around 34 psu) in the south. Both snapshots, and in particular the salinity one, demonstrate the fine horizontal resolution of the model by also showing the resolved submesoscale filaments and eddies abundant near the surface.

Finally, to illustrate the internal wave field resolved by the model, snapshots of the zonal and vertical velocity at 56°S are shown in Figure 4 and a horizontal section of vertical velocity at 2-km depth is shown in Figure 5. While the overall zonal velocity field (Figure 4a) is dominated by the surface-intensified

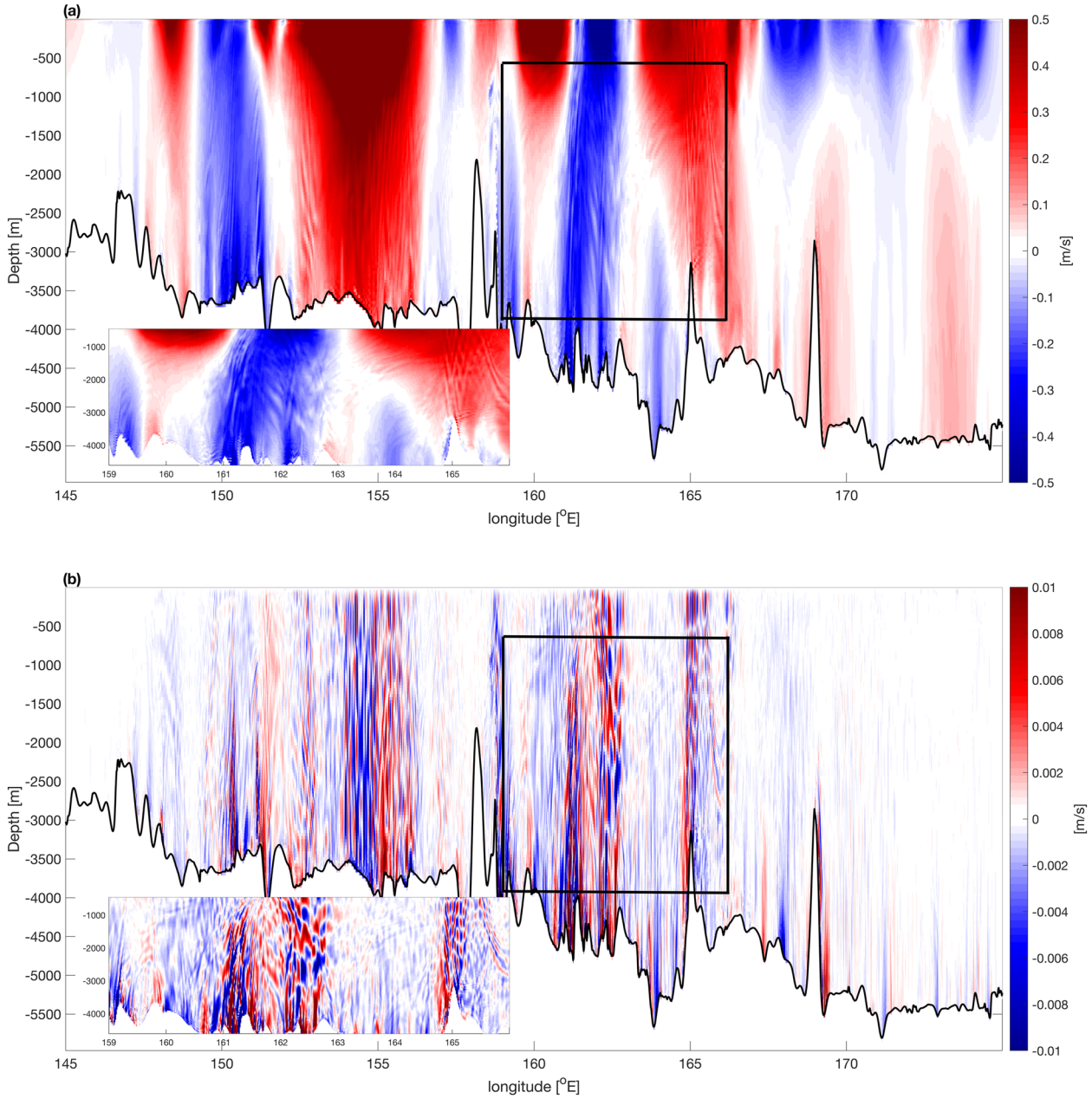

Figure 4. A snapshot of (a) zonal velocity and (b) vertical velocity in (m s^{-1}) at 56°S from the reference experiment. Embedded plot is a region shown with thick black line plotted with a more realistic aspect ratio.

mesoscale eddies with the surface velocities up to 0.5 m s^{-1}, small-scale internal waves can be seen in the deep ocean over the small-scale rough bottom topography in regions where strong eddy velocities reach the bottom. The internal waves are more apparent in the vertical velocity section (Figure 4b), which naturally filters out mesoscale eddies characterized by small vertical velocity. The internal wave motions extend a few kilometers above the bottom and can be identified as internal lee waves generated by the bottom flow over rough small-scale topography. In addition, the horizontal section of the vertical velocity (Figure 5) shows the horizontal distribution of internal waves in this region. They are distributed over regions of small-scale topography and mainly concentrate along the path of the ACC upstream and downstream of the Macquarie Ridge. Internal lee waves have horizontal scales of a few kilometers and vertical scale of 100–1,000 m and tend to radiate upward away from topography.

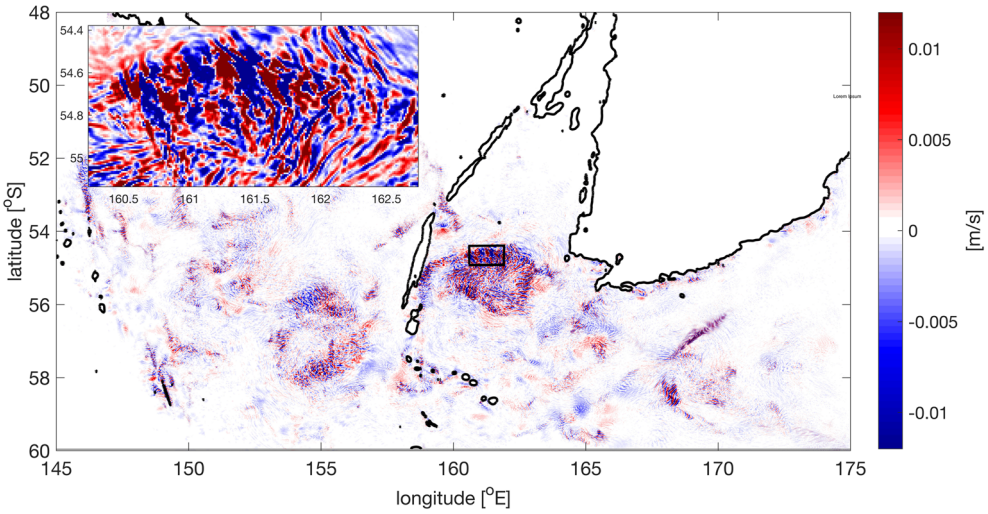

Figure 5. A snapshot of vertical velocity in (m s^{-1}) at 2,000-m depth from the reference experiment. Embedded plot is a region shown with thick black line plotted with a more realistic aspect ratio.

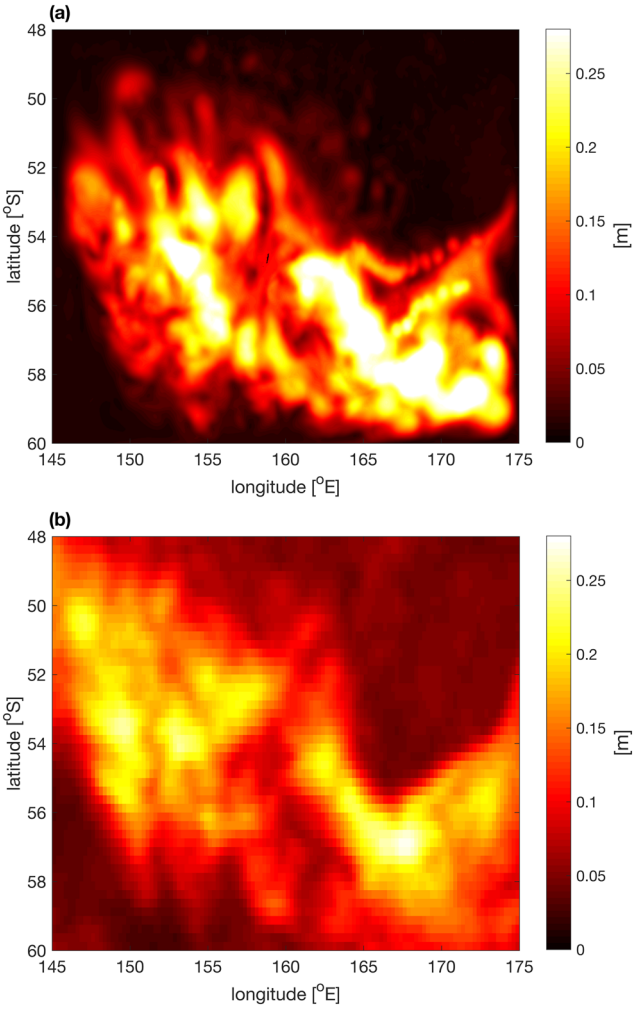

Figure 6. Standard deviation of the sea surface height in (m) from (a) 1/80° reference model and (b) satellite altimetry.

To validate the circulation features captured by our model, we compare the model outputs with observations. Since this model is forced by the annual-mean boundary conditions from SOSE and the model domain is fairly small (30° × 12°), the simulation is strongly constrained by the SOSE open boundary conditions. Therefore, the overall patterns of large-scale temperature and salinity distribution and circulation agree well with those from SOSE (not shown), which, in turn, is constrained by observations. On the other hand, our fine-resolution model also simulates transient mesoscale eddies, which are not directly constrained by the SOSE boundary conditions. To validate those, in Figure 6 we show standard deviation of the sea surface height anomaly from the reference simulation alongside that from satellite altimetry, which is the combined processing of Ocean Topography Experiment TOPEX/Poseidon and European Remote Sensing ERS-1 and ERS-2 (e.g., Marshall et al., 2006). Highly variable sea surface area along the path of the SAF is separated by the Macquarie Ridge, where flow instability is suppressed when the current flows through the narrow gap between the ridges (Rintoul et al., 2014). The model outputs roughly agree with the observations, though the model shows slightly higher variability than observed, which could be a result of much higher resolution of this model since the horizontal resolution of satellite data is 1/4°. Time-mean features of the local circulation are also validated by comparing the sea surface height in the model with the Mean Dynamic Topography (1993–2012) from the CNES-CLS13 product (Rio et al., 2011) distributed by AVISO (Figure 7). The comparison shows that the model captures the overall features of the horizontal circulation with a distinctive meander upstream of the Macquarie Ridge. The details of the meander vary between the model and observations likely due to a shorter averaging period used for the model results.

3.1.1. Topographic Form Stress

The TFS generated in the reference simulation with the unmodified SRTM30 topography is shown in Figure 8a. Positive values of the form stress correspond to acceleration, while negative values

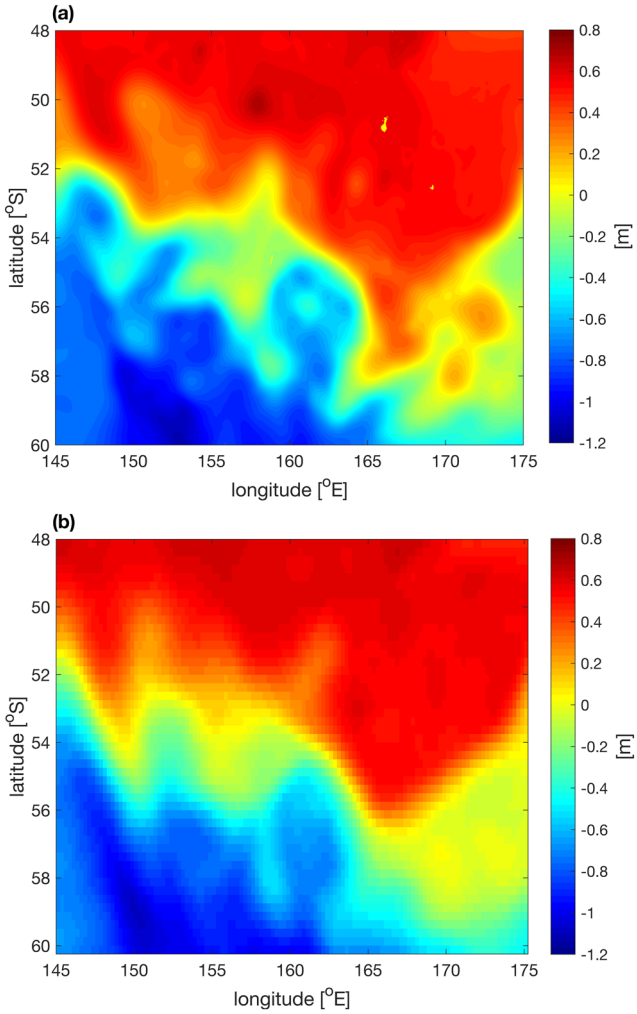

Figure 7. (a) Time-mean sea surface height in (m) from 1/80° reference model and (b) 1993–2012 Mean Dynamic Topography in (m) from the CNES-CLS13 product.

corresponds to deceleration in the zonal momentum balance. The distribution of the TFS is dominated by large-scale topographic features: the shape of the Macquarie Ridge and the Campbell Plateau can be clearly recognized. There are also numerous smaller spots of high form stress of both signs seen over small-scale topography regions upstream and downstream of the Macquarie Ridge. We can see that the largest negative TFS concentrates near the Macquarie Ridge, while the strong positive form stress values mainly occur over small topography accompanied by the comparable in magnitude and size negative areas near them. The pairs of positive and negative TFS can be also generated by a pressure difference across narrow troughs and ridges in the region south of the Macquarie Ridge at 56–58°S. Large-scale TFS shows a pattern consistent with the results from Masich et al. (2015). The small-scale TFS is generated with magnitudes as big as those of the large-scale form stress in this model. However, it mainly comes in pairs with different signs, resulting in a minor net effect in the zonal integral (Figure 9), consistent with the flow meandering north and south. In general, topographic features in this region apply strong positive and negative stress to the mean flow locally, but with predominantly a net negative stress against the mean flow in the zonal integral.

In terms of the time variability of the form stress, both large- and small-scale TFS show considerable variability as shown in Figure 10a. The TFS standard deviation is higher than the time-mean form stress. Largest variance appears over the Macquarie Ridge and abyssal hill regions upstream and downstream of it, while the form stress generated by the Campbell Plateau has relatively low variability. Our results are consistent

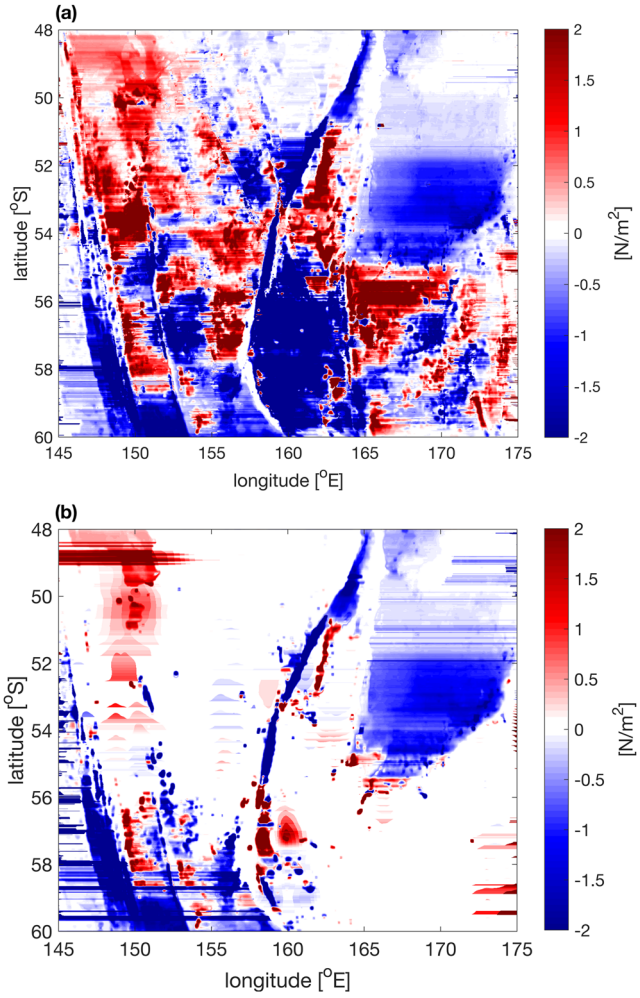

Figure 8. Time-mean topographic form stress in (N m^{-2}) from (a) rough topography experiment and (b) smooth topography experiment.

with those presented by Masich et al. (2015) and extend them to the variability of the small-scale TFS. Masich et al. (2015) suggested that the regions with narrow ridges, where the flow goes over and through, have highly concentrated and variable TFS, while the large bulk barriers, where flow goes around, have high mean form stress, but with low variability. Our results show that the form stress associated with abyssal hill topography is also characterized by strong variability, implying that it might have significant impact on transient circulation in this region such as flow meanders and eddies.

3.2. Simulation Without Small-Scale Topography

Topography plays an important role in the dynamical balance of the ACC as it can exert a form stress on the flow through the generation of the cross-topography pressure gradient. Therefore, we evaluate the direct impact of small-scale topography on the dynamical balance of the ACC by examining the changes of the TFS and the local circulation after removing the small-scale topography.

3.2.1. Time-Mean Topographic Form Stress

Time-mean TFS from the simulations with and without small-scale topography is shown in Figure 8. We can see that removing small-scale bottom topography in the deep ocean has little impact on the TFS at major large-scale topographic features such as the Campbell Plateau and the Macquarie Ridge. Notable negative TFS is mainly distributed in the south of the Campbell Plateau and along the elongated Macquarie Ridge. However, strong positive and negative TFS signals associated with small-scale topography upstream and downstream of the Macquarie Ridge largely disappear in the simulation without small-scale topography.

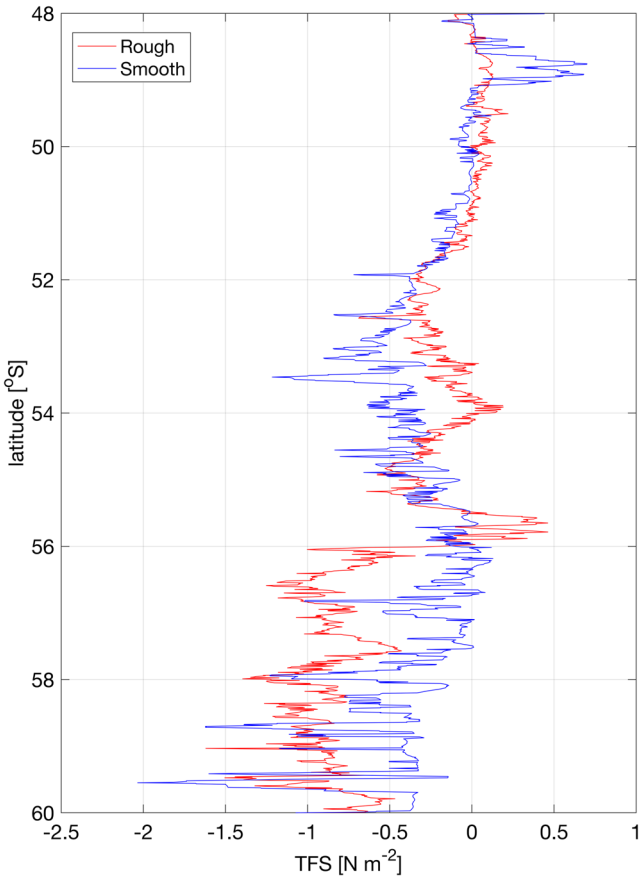

Figure 9. Zonal-mean topographic form stress in (N m^{-2}) from (red) rough topography experiment and (blue) smooth topography experiment.

The zonal integral of this form stress is shown in Figure 9. For lower latitudes in this domain (48–52°S), zonal-mean TFS is quite similar between the two experiments. The deceleration effect is enhanced only by about 10% in the absence of small-scale topography. On the contrary, at latitudes south of 56°S, the smooth topography simulation shows reduced magnitude of the negative form stress, or weakened ability of arresting the mean current. This reduction is likely due to the positive form stress associated with the trough to the south of Macquarie Ridge. This trough in the rough topography simulation is removed along with abyssal hills by the smoothing method in the smooth topography simulation. In general, the small-scale abyssal hill topography has a rather small effect on the zonally averaged form stress, compared to its local effect.

Although significant local changes occur after the removal of small-scale topography, most small-scale TFS values appear in pairs (positive and negative), and hence, they tend to cancel out after taking the zonal mean of this form stress. The dominant momentum sink for large-scale circulation in this region is still associated with large-scale features, especially the Macquarie Ridge. Meridionally elongated large-scale topography of the ridge contributes most effectively to the deceleration of the mean flow.

3.2.2. Time-Mean Circulation

To illustrate the response of the local circulation to changes in small-scale topography, in Figure 11 we show the time-mean sea surface height and its relation to the underlying TFS from the two simulations. We can see that there are significant changes in the local circulation around 155°E, where most of the changes in the TFS occurs upstream of the Macquarie Ridge. In this region, the mean flow in the rough topography simulation splits into two fronts that meander before they go around the Macquarie Ridge. In the smooth topography simulation, the local circulation is significantly changed. The curvature of these meanders upstream of the Macquarie Ridge is reduced. As the flow goes across small-scale topography in the rough topography simulation, it tends to flex southward with positive form stress and northward with negative

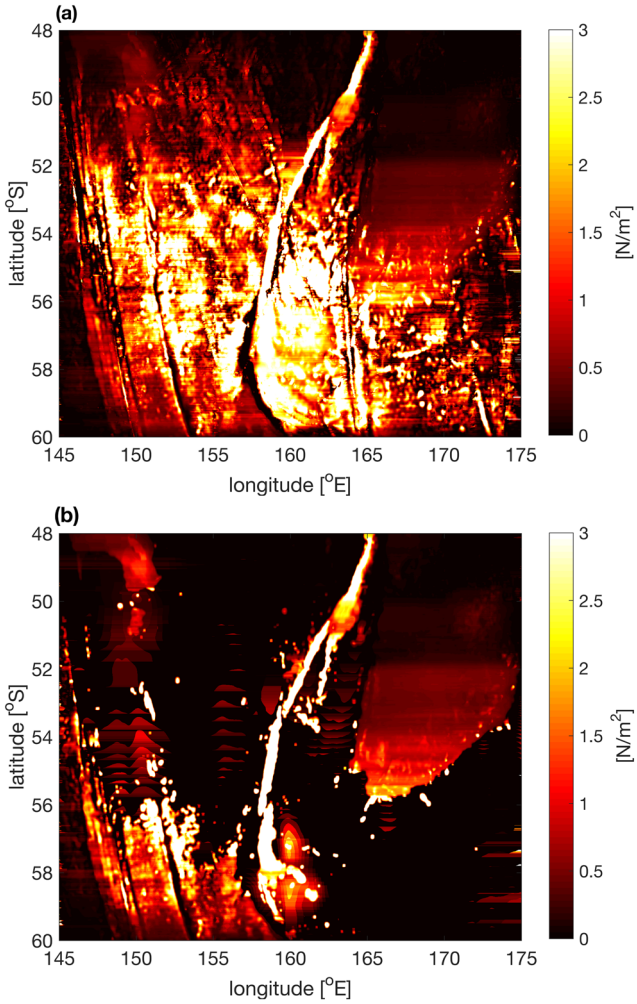

Figure 10. Standard deviation of topographic form stress in (N m^{-2}) from (a) rough topography experiment and (b) smooth topography experiment.

form stress. In the smooth topography simulation, on the other hand, most of the flow does not split into two fronts and does not meander upstream of the Macquarie Ridge. Instead, it continues straight to the ridge and then flows northward to cross the ridge through the gap at around 53°S. This response of the local circulation may be explained by the lack of small-scale topography, and hence local TFS, in the smooth topography simulation to balance the downward momentum transfer facilitated by the flow meanders (Thompson & Naveira Garabato, 2014). This leads to the re-organization of the flow with the reduction of the local meanders and the shift of the flow further downstream to the Macquarie Ridge, where the momentum can be removed by the TFS associated with the Macquarie Ridge. This explanation is consistent with an increase in magnitude of the mean negative TFS at 52–54°S associated with the Macquarie Ridge in the smooth topography simulation shown in Figure 9. Similarly, the meander south of the Campbell Plateau around 164°E is also weaker in the smooth simulation which might be due to the removal of the topographic trough south of the Campbell Plateau.

From a vertical perspective, the mean kinetic energy profile (Figure 12a) illustrates changes in the vertical structure of the time-mean flow. Consistently, mean kinetic energy is notably increased in the interior of the ocean (from 1,000 to 4,000 m under surface) in the smooth topography simulation, while it slightly decreases at the surface. As a result, the mean flow becomes more barotropic without small-scale topography.

Although the difference in the TFS between the two simulations appears to be less significant from a zonally averaged perspective, the meridional shift of the ACC meanders potentially has a large-scale impact through its effect on temperature and salinity distribution. The ACC fronts tend to shift poleward in the presence of

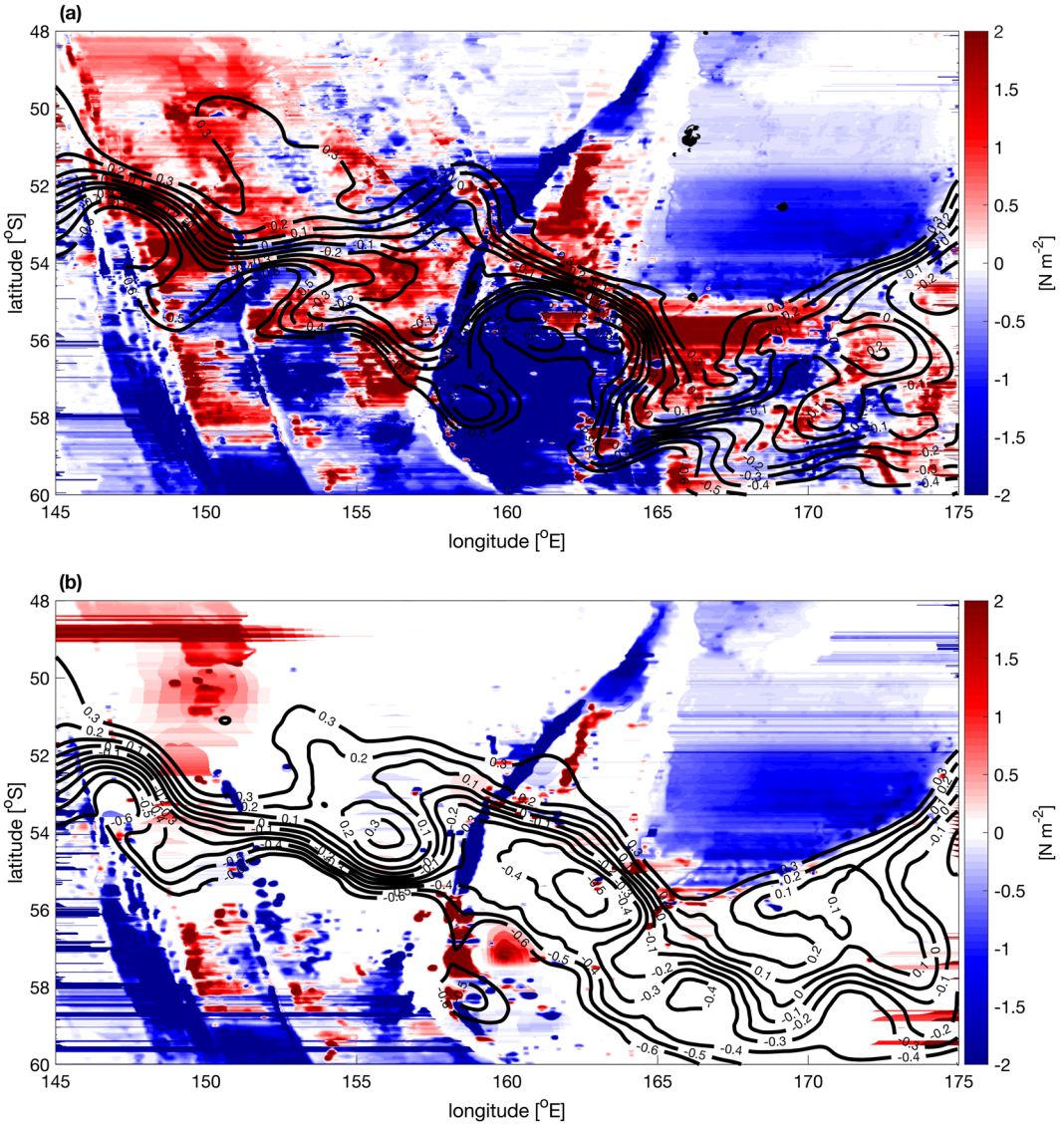

Figure 11. Time-mean topographic form stress in (N m^{-2}) and sea surface height contours from (a) rough topography and (b) smooth topography simulation.

small-scale topography, carrying warm water to the south. As the Ross Gyre is just south of our regional model domain, the ACC fronts shifting south may interact with the gyre thereby exerting effects on the ocean large-scale circulation. This could also be relevant to some other regions of the Southern Ocean where the ACC interacts with subpolar gyres as described in Wang et al. (2016).

In addition, the vertical profiles of the horizontally averaged TFS in these two simulations (Figure 13) show that in the upper ocean (from surface to 4-km depth) where the TFS is dominated by the large-scale topography, TFS is negative and its magnitude is not sensitive to the removal of the small-scale topography. On the other hand, for the abyssal ocean deeper than 4 km, TFS in the simulation without abyssal hills decreases by around 50% and becomes positive, consistent with Masich et al. (2015), in which the abyssal TFS was found to play a minor role in terms of momentum sink. However, in the Rough simulation, the abyssal TFS is comparable with the TFS in the upper ocean, indicating that the small-scale TFS is still dynamically important.

3.2.3. Variability

To describe the impact of small-scale topography on the variability of the flow, we diagnose the standard deviation of TFS and show it in Figure 10. We can see that the variance of TFS over the Macquarie Ridge is high and over the Campbell Plateau is low in both simulations, which is consistent with the results in

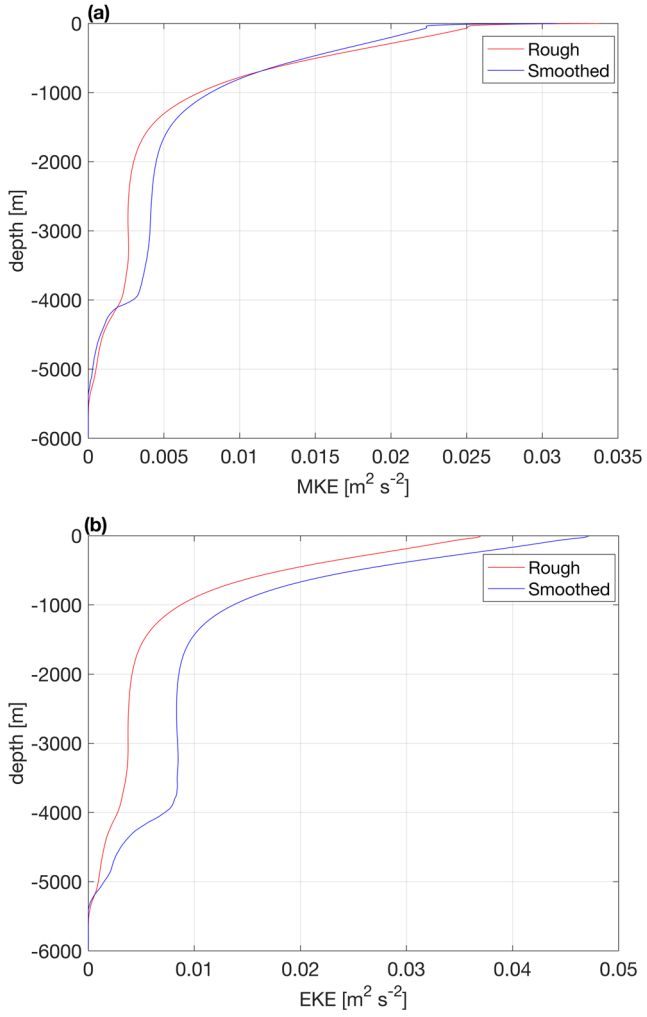

Figure 12. Vertical profiles of (a) mean kinetic energy in ($m^2\ s^{-2}$) and (b) time-mean eddy kinetic energy in ($m^2\ s^{-2}$) from (red) rough bottom topography and (blue) smooth bottom topography simulations.

Masich et al. (2015). The small-scale topography areas adjacent to Macquarie Ridge are of high variability in the rough topography simulation. This variability nearly all disappears when we remove the small-scale topography.

Given this strong variability of the TFS and its sensitivity to small-scale topography, we evaluate changes in the eddy field by calculating the EKE for both experiments. The surface and 3,500-m-deep time-mean EKE are shown in Figures 14 and 15. Except for the Campbell Plateau, the flows are highly variable and energetic throughout the whole domain and especially upstream and downstream of the Macquarie Ridge in both simulations. The EKE is enhanced after removing small-scale topography, which is clearly seen both at the surface and in the deep ocean, while the enhancement is greater in the deep ocean. In some regions, for example, northwest area at the surface (Figure 14), EKE has increased by up to a factor of 10. For the deep ocean (Figure 15), EKE around the Macquarie Ridge spreads to the north, leading to an order of magnitude EKE increase in the northern part of the domain. EKE has also greatly enhanced in the eddy hotspots upstream and downstream of the Macquarie Ridge.

Vertical sections of EKE are also plotted in Figure 16. In the rough topography simulation, EKE is stretched from the surface to the bottom around the meander region, 150–155°E, consistent with the similar pattern from a global ocean model described in Thompson and Naveira Garabato (2014). For the smooth topography simulation, besides the even higher deep ocean EKE than that in the rough topography simulation, deep ocean eddy activity is also enhanced in other regions such as on the eastern flank of the ridge and the

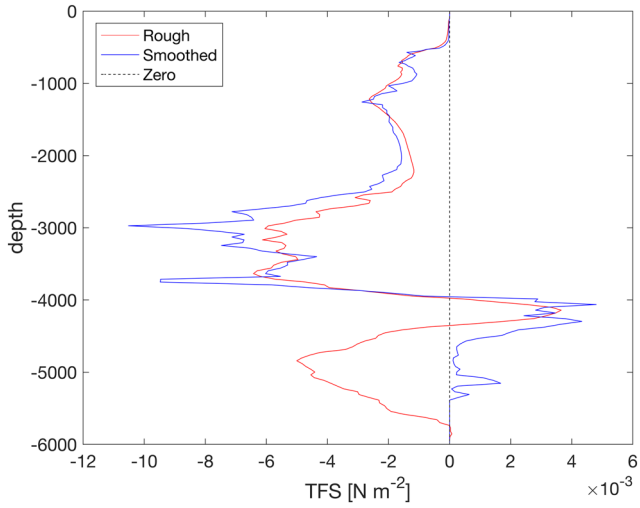

Figure 13. Vertical profile of horizontally averaged topographic form stress (N m^{-2}) in rough simulation (red) and smooth simulation (blue).

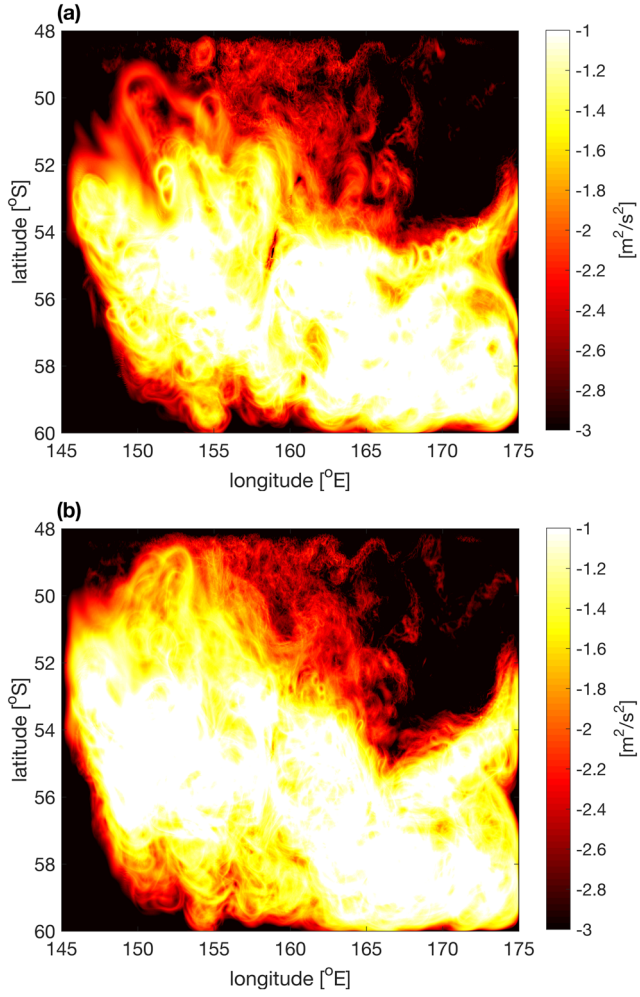

Figure 14. Time-mean EKE in $\log_{10}(m^2\,s^{-2})$ at the surface from (a) rough topography and (b) smooth topography simulation.

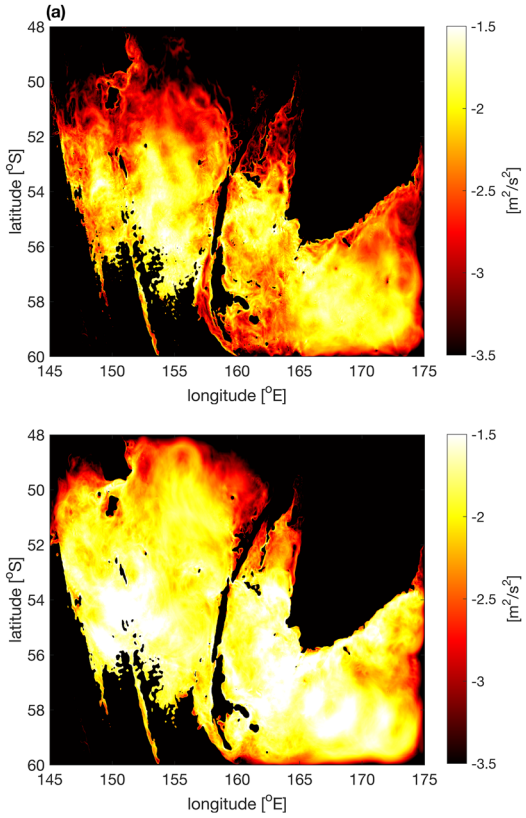

Figure 15. Time-mean EKE in $\log_{10}(m^2\ s^{-2})$ at 3,500-m depth from (a) rough topography and (b) smooth topography simulation.

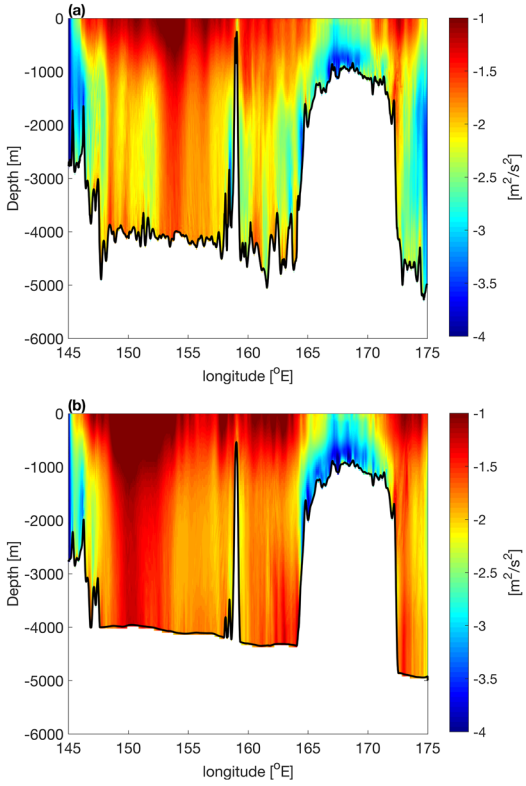

Figure 16. Time-mean EKE in $\log_{10}(m^2\ s^{-2})$ at 54°S from (a) rough topography and (b) smooth topography simulation.

eastern area of the Campbell Plateau with both of them showing at least an order of magnitude EKE increase. This vertical EKE comparison demonstrates the impact of small-scale topography on the extraction of eddy energy near the bottom and hence the impact on their vertical structure.

Unlike the mean flow kinetic energy (Figure 12a), which varies more significantly in the ocean interior than at the surface, the eddy field is more energetic in the absence of small-scale topography both in the interior and at the surface of the ocean (Figure 12b). Although the eddy activities are strengthened both at the surface and in the deep ocean, the spatially averaged surface EKE is increased by 20%, while the deeper ocean (from 2,000 to 4,000 m) EKE is elevated by a factor of 2 in the simulation without small-scale topography. This reveals that small-scale topography impacts not only the time-mean circulation at depth but also the time-varying eddy field.

4. Discussion and Conclusions

Small, O(1–100 km), scale abyssal hill topography has been suggested by theoretical studies and idealized numerical models to play an important role in the dynamical balance of the ACC and the ocean circulation through the generation of internal waves, topographic wakes, and other low-level nonlinear motions. However, its impact has not been simulated in large-scale circulation models explicitly due to model resolution limitation. We carry out fine-resolution regional simulations, and our results show that small-scale topography makes a significant contribution to the TFS and impacts both time-mean and time-varying flows in the Southern Ocean. Below, we provide our interpretation and explanation of the results based on previous theories and simulations. The understanding of the role played by small-scale topography in the dynamical balance of the ACC that we offer is complementary to the mechanism of the local dynamics and the ACC response to changes in wind suggested by Thompson and Naveira Garabato (2014).

Abyssal hills with horizontal scales of 1–100 km are ubiquitous features of the seafloor and have been recognized as the predominant scale for generating internal waves in the abyssal ocean. These waves can radiate away and dissipate, thereby extracting energy and momentum from the background flow by applying internal wave drag (e.g., Naveira Garabato et al., 2013). When flow passes over an obstacle, internal lee waves are generated, and this wave generation is accompanied by the pressure gradient across topography. This pressure gradient results in the TFS, which is equivalent to wave drag near topography (Bell, 1975). Flows going around an obstacle can also generate evanescent internal waves, topographic wake eddies, and other turbulent motions. When these motions dissipate, there is also an associated drag, or TFS, that will act against the background flow to extract energy from it to sustain this dissipation (Klymak, 2018). Therefore, we take the TFS calculated from pressure difference across topography as an indicator of these processes to evaluate the role of small-scale topography for the dynamical balance of the ACC.

Changing the bottom topography instead of surface wind in our experiments and hence complementing the analysis and mechanism of Thompson and Naveira Garabato (2014), we show that flow meanders, facilitating the transfer of momentum downward, depend not only on the wind imparting momentum at the surface but also on the bottom topographic roughness removing this momentum from the flow. It is found that the curvature of the surface meanders around 152°E and 154°E is reduced in the absence of small-scale topography. Based on the kinetic energy profiles (Figure 12), we suggest that the small-scale topography has stronger impact on the deep circulation, which can be explained as the response to a reduced extraction of energy from the background flow exerted by small-scale TFS. This is consistent with the understanding that the surface circulation (i.e., the ACC meanders) are set to transfer momentum input by wind (fixed in our models) downward to balance it by TFS. Therefore, when the small-scale topography is removed, roughly the same momentum is transferred to the bottom, but it is not removed as efficiently and hence results in stronger bottom flows.

In the absence of small-scale topography, the ACC fronts also tend to shift equatorward. Similar meridional shift of the fronts is investigated in Wang et al. (2016), where they show that, in response to the removal of Kerguelen Plateau (KP), the Indian Ocean part of the ACC shifts poleward, which leads to a warm anomaly in the upper North Atlantic and the corresponding decrease of the North Atlantic Deep Water (NADW) formation. In addition, their results indicate that the southward shift of the ACC in the no-KP simulation makes the Weddell Gyre warmer and saltier, which reduces the formation of Antarctic Bottom Water (AABW), thereby influencing the global thermohaline circulation. In our study, the meridional shift of the ACC fronts is significant between the simulations with and without small-scale topography, and

hence, it is possible that the small-scale topography may also have an impact on the large-scale circulation. However, our model is regional, and large-scale responses cannot be directly explored. This effect can be addressed in future studies.

For the time-varying flows, the surface and abyssal ocean EKE maps and vertical sections show that eddies become more vigorous without small-scale topography. EKE is generated through the instability of large-scale currents and is dissipated in the Southern Ocean primary through the interaction with bottom topography. Hence, the absence of small-scale topography allows a buildup and enhancement of EKE in the deep ocean without being dissipated by the interaction with small-scale topography.

The vertical profiles of mean kinetic energy indicate that the mean flow becomes more barotropic without small-scale topography. This result complements the discussion of the barotropic/baroclinic partitioning of the circulation in Peña-Molino et al. (2014). Using an eddy-permitting model of the Southern Ocean, they found that, while flows in the Southern Ocean are mainly baroclinic in the center of ocean basins, the proportion of the barotropic transport increases near the large-scale topography. Our results suggest that away from large-scale topography this partitioning may also be influenced by small-scale abyssal hills, which facilitate the flow dissipation and hence regulate the strength of the bottom flow.

Acknowledgments

This research was undertaken on the NCI National Facility in Canberra, Australia, which is supported by the Australian Government. M. N. is grateful for the support from the Australian Research Council Discovery Project (DP170102162). The data used in this study are available through the NCI National Facility (project ds0 at raijin.nci.org.au) or upon request from the authors. We also thank Matthew Mazzloff and an anonymous reviewer for their comments and suggestions.

References

Becker, J., Sandwell, D., Smith, W., Braud, J., Binder, B., Depner, J., et al. (2009). Global bathymetry and elevation data at 30 arc seconds resolution: SRTM30_PLUS. *Marine Geodesy*, *32*(4), 355–371.

Bell, T. (1975). Topographically generated internal waves in the open ocean. *Journal of Geophysical Research*, *80*(3), 320–327.

Böning, C. W., Dispert, A., Visbeck, M., Rintoul, S., & Schwarzkopf, F. U. (2008). The response of the Antarctic Circumpolar Current to recent climate change. *Nature Geoscience*, *1*(12), 864.

Gill, A., & Bryan, K. (1971). Effects of geometry on the circulation of a three-dimensional southern-hemisphere ocean model. In *Deep Sea Research and Oceanographic Abstracts* (Vol.18, pp. 685–721). Great Britain: Pergamon Press.

Gille, S. T. (1997). The Southern Ocean momentum balance: Evidence for topographic effects from numerical model output and altimeter data. *Journal of Physical Oceanography*, *27*(10), 2219–2232.

Gordon, A. L. (1972). On the interaction of the Antarctic Circumpolar Current and the Macquarie Ridge. *Antarctica Oceanology II: The Australian-New Zealand Sector*, *19*, 71–78.

Hughes, C. W. (2005). Nonlinear vorticity balance of the Antarctic Circumpolar Current. *Journal of Geophysical Research*, *110*, C11008. https://doi.org/10.1029/2004JC002753

Ivchenko, V. O., Richards, K. J., & Stevens, D. P. (1996). The dynamics of the Antarctic Circumpolar Current. *Journal of Physical Oceanography*, *26*(5), 753–774.

Ivchenko, V., & Stevens, D. (1995). The zonal momentum balance in a realistic eddy resolving general circulation model of the Southern Ocean. *Journal of Physical Oceanography*, *26*, 753–774.

Jackett, D. R., & Mcdougall, T. J. (1995). Minimal adjustment of hydrographic profiles to achieve static stability. *Journal of Atmospheric and Oceanic Technology*, *12*(2), 381–389.

Killworth, P. D., & Nanneh, M. M. (1994). Isopycnal momentum budget of the Antarctic Circumpolar Current in the Fine Resolution Antarctic Model. *Journal of Physical Oceanography*, *24*(6), 1201–1223.

Klymak, J. (2018). Non-propagating form drag and turbulence due to stratified flow over large-scale abyssal hill topography. *Journal of Physical Oceanography*, *48*, 2383–2395.

Kunze, E., Firing, E., Hummon, J. M., Chereskin, T. K., & Thurnherr, A. M. (2006). Global abyssal mixing inferred from lowered ADCP shear and CTD strain profiles. *Journal of Physical Oceanography*, *36*(8), 1553–1576.

Marshall, J., Adcroft, A., Hill, C., Perelman, L., & Heisey, C. (1997). A finite-volume, incompressible Navier Stokes model for studies of the ocean on parallel computers. *Journal of Geophysical Research*, *102*(C3), 5753–5766.

Marshall, J., Olbers, D., Ross, H., & Wolf-Gladrow, D. (1993). Potential vorticity constraints on the dynamics and hydrography of the Southern Ocean. *Journal of Physical Oceanography*, *23*(3), 465–487.

Marshall, J., Shuckburgh, E., Jones, H., & Hill, C. (2006). Estimates and implications of surface eddy diffusivity in the Southern Ocean derived from tracer transport. *Journal of Physical Oceanography*, *36*, 1806–1821.

Mashayek, A., Ferrari, R., Merrifield, S., Ledwell, J. R., St Laurent, L., & Garabato, A. N. (2017). Topographic enhancement of vertical turbulent mixing in the Southern Ocean. *Nature communications*, *8*(14), 197.

Masich, J., Chereskin, T. K., & Mazloff, M. R. (2015). Topographic form stress in the Southern Ocean State Estimate. *Journal of Geophysical Research: Oceans*, *120*, 7919–7933. https://doi.org/10.1002/2015JC011143

Mazloff, M. (2005). Southern Ocean State Estimate (PhD thesis), MIT-WHOI Joint Program.

McWilliams, J. C., Holland, W. R., & Chow, J. H. (1978). A description of numerical Antarctic Circumpolar Currents. *Dynamics of Atmospheres and Oceans*, *2*(3), 213–291.

Munk, W. H., & Palmén, E. (1951). Note on the dynamics of the Antarctic Circumpolar Current. *Tellus*, *3*(1), 53–55.

Naveira Garabato, A. C., Nurser, A. G., Scott, R. B., & Goff, J. A. (2013). The impact of small-scale topography on the dynamical balance of the ocean. *Journal of Physical Oceanography*, *43*(3), 647–668.

Naveira Garabato, A. C. N., Polzin, K. L., King, B. A., Heywood, K. J., & Visbeck, M. (2004). Widespread intense turbulent mixing in the Southern Ocean. *Science*, *303*(5655), 210–213.

Nikurashin, M., & Ferrari, R. (2011). Global energy conversion rate from geostrophic flows into internal lee waves in the deep ocean. *Geophysical Research Letters*, *38*, L08610. https://doi.org/10.1029/2011GL046576

Peña-Molino, B., Rintoul, S., & Mazloff, M. (2014). Barotropic and baroclinic contributions to along-stream and across-stream transport in the Antarctic Circumpolar Current. *Journal of Geophysical Research: Oceans*, *119*, 8011–8028. https://doi.org/10.1002/2014JC010020

Rintoul, S. R., Hughes, C. W., & Olbers, D. (2001). The Antarctic Circumpolar Current system. *International Geophysics*, *77*, 271–XXXVI. Elsevier.

Rintoul, S. R., & Naveira Garabato, A. C. (2013). Dynamics of the Southern Ocean circulation. *International Geophysics*, *103*, 471–492. Elsevier.

Rintoul, S. R., Sokolov, S., Williams, M. J. M., Pema Molino, B., Rosenberg, M., & Bindoff, N. L. (2014). Antarctic Circumpolar Current transport and barotropic transition at Macquarie Ridge. *Geophysical Research Letters*, *41*, 7254–7261. https://doi.org/10.1002/2014GL061880

Rio, M. H., Guinehut, S., & Larnicol, G. (2011). New CNES-CLS09 global mean dynamic topography computed from the combination of GRACE data, altimetry, and in situ measurements. *Journal of Geophysical Research*, *116*, C07018. https://doi.org/10.1029/2010JC006505

Rosso, I., Hogg, A. M., Kiss, A. E., & Gayen, B. (2015). Topographic influence on submesoscale dynamics in the Southern Ocean. *Geophysical Research Letters*, *42*, 1139–1147. https://doi.org/10.1002/2014GL062720

Rosso, I., Hogg, A. M., Strutton, P. G., Kiss, A. E., Matear, R., Klocker, A., & van Sebille, E. (2014). Vertical transport in the ocean due to sub-mesoscale structures: Impacts in the Kerguelen Region. *Ocean Modelling*, *80*, 10–23.

Sandwell, D. T., & Smith, W. H. (2009). Global marine gravity from retracked GEOSAT and ERS-1 altimetry: Ridge segmentation versus spreading rate. *Journal of Geophysical Research*, *114*, B01411. https://doi.org/10.1029/2008JB006008

Scott, R. B., Goff, J. A., Naveira Garabato, A. C., & Nurser, A. J. G. (2011). Global rate and spectral characteristics of internal gravity wave generation by geostrophic flow over topography. *Journal of Geophysical Research*, *116*, C09029. https://doi.org/10.1029/2011JC007005

Sloyan, B. M. (2005). Spatial variability of mixing in the Southern Ocean. *Geophysical Research Letters*, *32*, L18603. https://doi.org/10.1029/2005GL023568

Thompson, A. F., & Naveira Garabato, A. C. (2014). Equilibration of the Antarctic Circumpolar Current by standing meanders. *Journal of Physical Oceanography*, *44*(7), 1811–1828.

Tulloch, R., Ferrari, R., Jahn, O., Klocker, A., LaCasce, J., Ledwell, J. R., et al. (2014). Direct estimate of lateral eddy diffusivity upstream of Drake Passage. *Journal of Physical Oceanography*, *44*(10), 2593–2616.

Wang, J., Mazloff, M. R., & Gille, S. T. (2016). The effect of the Kerguelen Plateau on the ocean circulation. *Journal of Physical Oceanography*, *46*, 3385–3396.

Wolff, J.-O., Maier-Reimer, E., & Olbers, D. J. (1991). Wind-driven flow over topography in a zonal β-plane channel: A quasi-geostrophic model of the Antarctic Circumpolar Current. *Journal of Physical Oceanography*, *21*(2), 236–264.

Yang, L., Nikurashin, M., Hogg, A. M., & Sloyan, B. (2018). Energy loss from transient eddies due to lee wave generation in the Southern Ocean. *Journal of Physical Oceanography*, *48*, 2867–2885.